Study of the SP-100 Radiator Heat Pipes Response to External Thermal Exposure

Mohamed S. El-Genk* and Jong T. Seo*
University of New Mexico, Albuquerque, New Mexico

This research presents the results of a study of the transient response of potassium heat pipes, simulating the SP-100 system radiator heat pipes, to external thermal exposure. Results demonstrate that a heat pipe failure caused by external thermal exposure below 200 kW/m^2 is unlikely; however, a reverse operation that will transport a fraction of the external heat to the lithium in the secondary coolant loop will occur temporarily. This fraction of the external heat increases with the heat flux, the exposed fraction of the heat pipe, and the exposure time up to the heat pipe's response time (~ 6.5 s). Beyond this time, the fraction of the external heat transported to the secondary coolant becomes independent of the exposure time. Conversely, the fraction of the external heat radiated into space decreases as the exposed fraction of the heat pipe and/or the heat flux increases. Results also demonstrate that a full external exposure as low as 17 kW/m^2 lasting for more than 6.5 s can reverse the operation of the radiator's heat pipes, regardless of their lengths. However, a full exposure of the radiator at its inward surface to a net heat flux of only 200 kW/m^2 for more than 6.5 s could cause the heat pipe wall to fail as the induced stress in the wall due to the vapor pressure of the potassium working fluid exceeds the yield strength of the titanium liner of the wall.

Nomenclature

F = radiation view factor
L = length, m
P = power, W
q'' = heat flux, W/m^2
T = temperature, K
t = time, s
x = exposed fraction
ϵ = surface emissivity

Subscripts
ex = external exposure
l = longest heat pipe
o = rejection by radiation
s = shortest heat pipe
ss = steady state

Introduction

THE SP-100 system, currently in the engineering design, development, and testing phase, employs a fast flux nuclear reactor, which delivers approximately 2.5 MW of thermal power. The reactor thermal energy is removed by liquid lithium circulating through the primary loops to the heat exchangers where it is transmitted to the SiGe/GaP thermoelectric (TE) converters.[1] The TE converters generate 100 kW of electric power while the liquid lithium in the secondary coolant loops transports the rest of the reactor thermal power to the radiator's heat pipes, where it is rejected into space. Both the primary and the secondary lithium coolants are circulated by thermoelectric-electromagnetic (TE-EM) pumps, with hiperco-27 self-induced magnets. As shown in Fig. 1, each pump services a primary and a secondary loop. The baseline design of SP-100 system calls for 12 subsystems, each consisting of a primary and a secondary loop, a TE-EM pump, a radiator panel, and a power conversion assembly (PCA). Each pair of primary and secondary loops is thermal-hydraulically coupled in the TE-EM pump and thermally coupled in the PCA. In both locations, the TE converters are sandwiched between the ducts of the primary lithium coolant (heat source) and the secondary lithium coolant (heat sink). Figure 1 diagrams the coupling of the primary and secondary coolant loops, whereas Fig. 2 presents a schematic of the SP-100 system's radiator heat pipes. As shown in Fig. 2, the SP-100 radiator consists of a total of 12 radiator panels; each panel is thermally coupled to a separate secondary coolant duct. The secondary coolant duct is laid longitudinally along the center of the panel, and is thermally coupled to the radiator panel heat pipes. These heat pipes, which have potassium working fluid and a foil etched annular wick, are laid at right angles to the secondary coolant ducts and are interconnected by beryllium fins. These fins are not only for structural strength but also increase the radiator's effective surface area. Each panel has 352 heat pipes. These heat pipes, whose lengths vary along the radiator panel, are arranged in two rows (176 heat pipes each); one row is thermally coupled to the duct of the incoming secondary coolant and the other to the duct of the returning secondary coolant. The longest heat pipe in the panel, located at the far end toward the payload, is 0.92-m long, whereas the shortest heat pipe, located at the near end toward the reactor system, is only 0.55-m long. To harden the radiator's heat pipes against natural and man-made debris while minimizing their thermal resistance, their walls are composed of a 152-μm titanium liner (melting point 1933K), a 330-μm beryllium overcoat (melting temperature 1551 K), and a 25-μm interfacial bonding layer of silver (melting point 1235 K). Also, the secondary coolant ducts are protected from micrometeorites by a rectangular beryllium enclosure (see Fig. 2). Although both sides of the radiator panel contribute to the rejection of the system's waste heat, the effective radiation view factor for the side facing inward will be lower than that for the side facing outward because of the conical shape of the radiator. Also, the effective emissivity, which depends on the surface temperature, will be different for each side.

A concern in the operation of the SP-100 system is understanding the transient response of a radiator heat pipe during an external heating of its surface. An important issue is

Received May 2, 1988; revision received Feb. 6, 1989.

*Institute for Space Nuclear Power Studies, Department of Chemical and Nuclear Engineering.

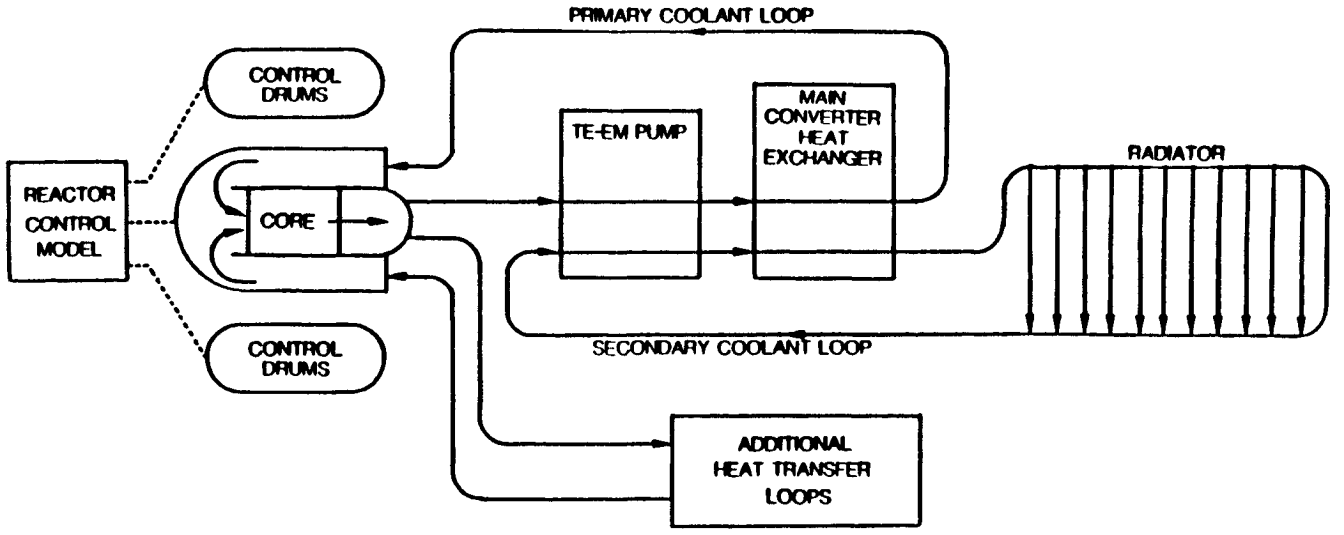

Fig. 1 Line diagram of the primary and secondary coolant loops in the SP-100 system.

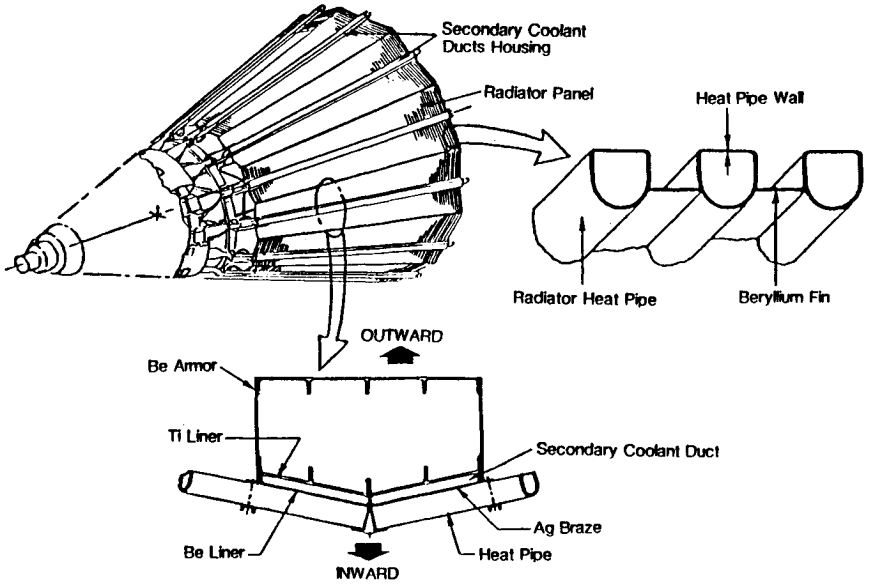

Fig. 2 Illustration of the coupling of the radiator panel's heat pipes to the secondary coolant ducts.

whether external heating can cause the radiator's heat pipes to fail. Failure may be caused by exceeding the heat pipe's boiling limit, by approaching the melting temperature of the silver bond, or by exceeding the yield strength of the titanium liner in the heat pipe wall during the transient. However, since the radiator's heat pipes are thermally coupled to the secondary lithium coolant, low external heating may only cause temporary operation of the radiator heat pipes in the reversed mode. In this mode of operation, heat pipes in the exposed area of the radiator will transport a fraction of the external heat to the secondary lithium coolant resulting in a lower electric power output for the system.

To address these issues, research investigating the transient response of a potassium radiator heat pipe to an external surface heating was conducted. This analysis used a circular-cross-section heat pipe to simulate the heat pipes in the SP-100 radiator panels. A parametric analysis was performed to assess the effects of varying the external heat flux, the exposed fraction of the heat pipe, the exposure time, and the total heat pipe length on the operation, as well as the transient response and vulnerability of the radiator's heat pipes. This analysis was conducted using a two-dimensional transient model for liquid metal heat pipes.[2-4] The following section briefly describes this transient heat pipe model.

Description of Two-Dimensional Transient Model for Liquid Metal Heat Pipes

The general features of the transient heat pipe model are outlined in Table 1. The model solves the two-dimensional (r,z) transient energy equation in the wall region, and the transient energy, mass, and momentum conservation equations in the liquid region. Because the vapor hydraulic time ($\sim 10^{-3}$ s) is approximately two orders of magnitude smaller than the liquid characteristic time (~ 0.1 s), the transient operation of the heat pipe will be limited by the latter and a quasi-steady-state, one-dimensional approximation can be used to solve the energy, mass, and momentum conservation equations in the vapor region. The vapor hydraulic time is defined as the time required for the vapor to travel the length of heat pipe at the sonic velocity, and the liquid characteristic time is equal to the square of the thickness of the liquid layer divided by the thermal diffusivity of the liquid. Recently, Bowman and Hitchcock's[5] experiment demonstrated that the vapor in the

heat pipe can be accurately modeled using the steady-state governing equations.

As indicated in Table 1, the thermophysical properties of both the liquid and vapor phases are allowed to vary with temperature, but a completely thawed heat pipe is assumed. This model also assumes that no noncondensible gas is present in the vapor core and a perfect wetting occurs between the wick material and working fluid (i.e., the wetting angle is zero). The model employs an annular-type wick structure covered by a screen mesh; however, other wick structures can easily be incorporated. The constituent equations in the wall, liquid, and vapor regions of the heat pipe, with the appropriate boundary and the initial conditions, are solved simultaneously using the implicit finite-difference method. The coupling of the energy and momentum equations in the liquid and vapor regions enables the model to predict the operation limits of the heat pipe during steady-state and transient operation. The operation limits simulated in the model include the sonic, entrainment, capillary, and boiling limit.[2,4] The advantages of this model over previous models reported in the literature[6-11] include incorporating temperature-dependent thermophysical properties, and the capability of treating various combinations of boundary conditions at the evaporator and the condenser regions, as well as predicting the operation limits of the heat pipes during both steady-state and transient operation. More details on the model development can be found elsewhere.[2,4] The next section discusses the results of model verification by comparing with experimental data.

Model Verification

To verify the results of the two-dimensional heat pipe model, its predictions were compared with the experimental data for a cooldown transient of a lithium heat pipe.[12] The model predictions of the temperature distribution in the various heat pipe regions, except at the end of the condenser region, were in agreement with the experimental data.[2] Before shutdown, the heat pipe was operating at 1250 K evaporator exit temperature with 15-kW power throughput. As shown in Fig. 3a, the model predictions of the axial temperature distribution in the heat pipe, when the lithium in the condenser reached its freezing temperature of 454 K, were in good agreement with the experimental data except at the end of the condenser region. In this region, the measured temperature remained much higher than the freezing temperature of the lithium because of the pooling effect caused by the excess working fluid in the heat pipe.[12] Figure 3b also shows that the model prediction of the cooldown time of the heat pipe of 548 s was only 38 s longer than the reported time in the experiment.[12] Although this comparison of the model predictions with the experimental data is limited, the results suggest that the modeling approach and the assumptions introduced during the model development are sound. However, additional verification of the model using other transient experimental data, whenever available, is highly recommended. In the next section, the transient heat pipe model is used to investigate the transient response and examine the vulnerability of a radiator heat pipe to an external thermal exposure.

Table 1 Description of transient model for liquid metal heat pipes

Physical model descriptions
1. Equations solved:
Transient wall energy equation
Transient liquid energy, mass, and momentum conservation equations
Steady-state vapor energy, mass, and momentum conservation equations
Mass and energy equations of the liquid and vapor are coupled through the evaporation/condensation at the interface
Momentum equations of the liquid and vapor are coupled through the capillary pressure relationship of the wick
2. Geometry and dimensions:
Cylindrical coordinate
Two-dimensional (axial and radial) for the wall and liquid regions
One-dimensional (axial) for the vapor region
3. Heat pipe phenomenological models:
The evaporation/condensation at the liquid–vapor interface is governed by the heat balance
Capillary pressure relationship based on the vapor volume fraction and temperature dependent surface tension
4. Numerical method:
Implicit finite-difference method
5. Capabilities:
Handle any combination of constant or time-dependent boundary conditions at the evaporator and condenser regions (temperature, heat flux, convection, and radiation)
Predicts the heat pipe operation limits for steady-state and transient operation
Assumptions
1. Quasisteady-state model for the vapor region
2. No noncondensible gas
3. Good wettability between wick and working fluid
4. Temperature-dependent thermophysical properties
Remarks
1. It is designed to be fast running for incorporation in an integrated SP-100 system model, SNPSAM
2. The model simulates reversed operation of heat pipes; a feature that is desirable for the survivability studies of the SP-100 system

Method of Analysis

The transient heat pipe model described in the previous sections was used to investigate the effect of an external ther-

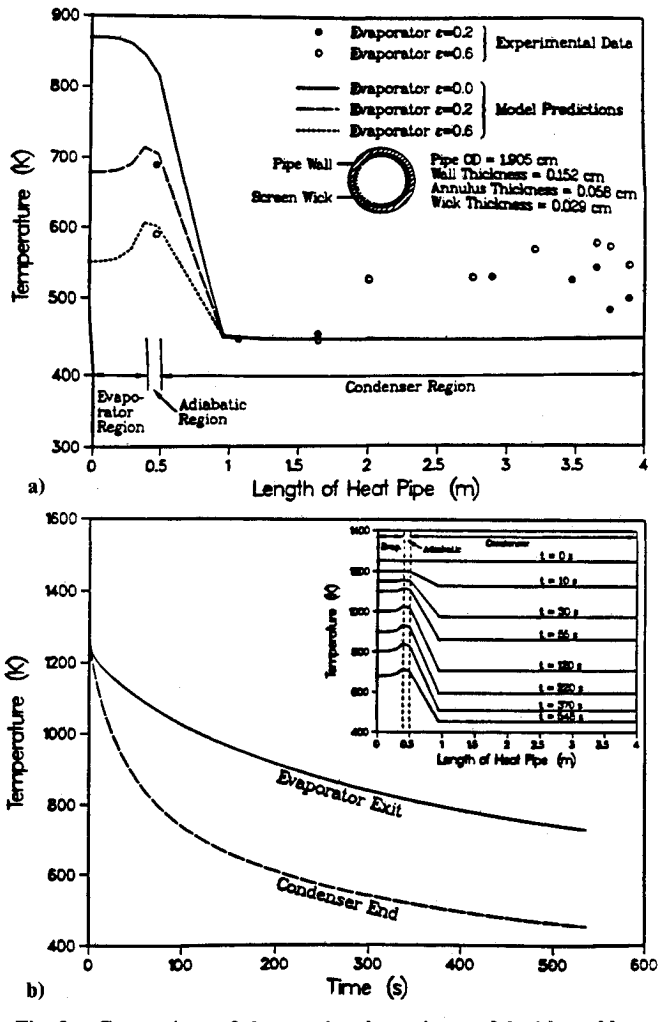

Fig. 3. Comparison of the transient heat pipe model with cooldown experimental data of a lithium heat pipe: a) temperature distribution in the heat pipe and b) evaporator and condenser temperatures and temperature distributions as functions of time.

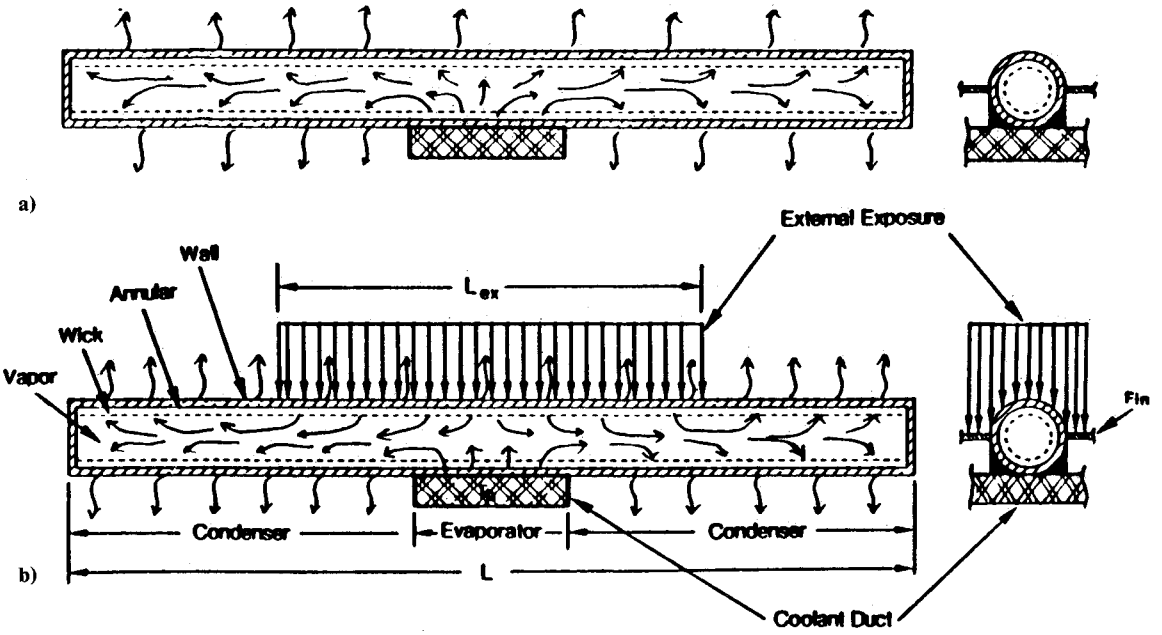

Fig. 4 Schematics simulating a radiator heat pipe during a) normal operation and b) exposure to external heating.

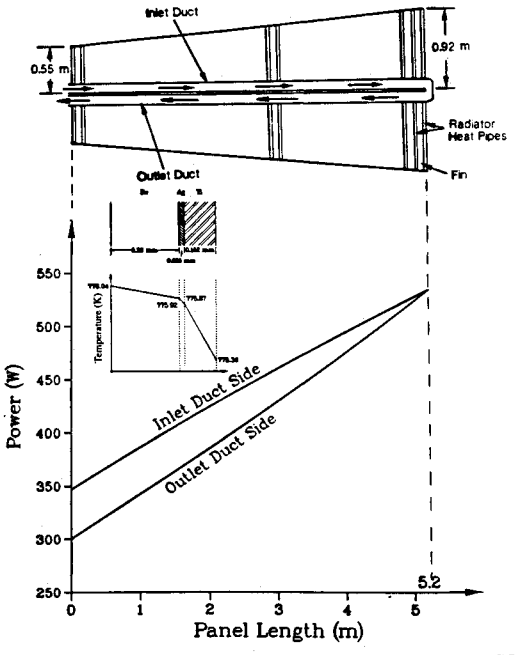

Fig. 5 Calculated power throughputs of the heat pipes in SP-100 radiator panel during normal operation of the SP-100 system at 100 kWe.

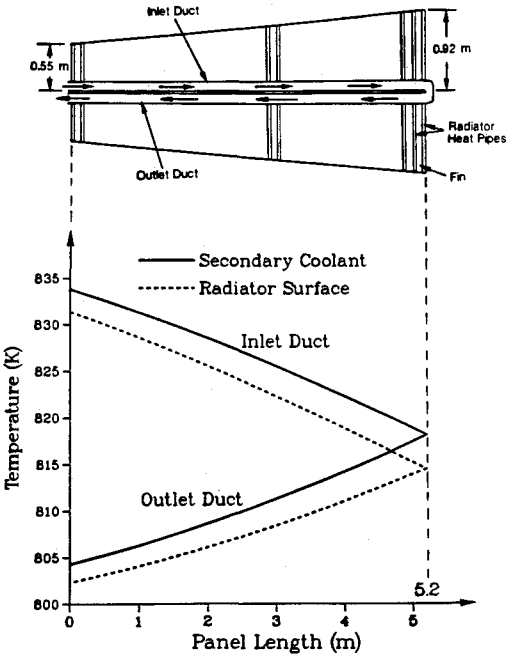

Fig. 6 Calculated temperatures of the secondary lithium coolant and the radiator heat pipes during normal operation of the SP-100 system at 100 kWe.

mal exposure on the operation of a liquid metal heat pipe simulating those in the SP-100 system's radiator. As illustrated in Fig. 2, the cross section of the radiator's heat pipes in the SP-100 system is noncircular, the heat pipes are interconnected with metallic fins, and the heat input to the evaporator region is not azimuthally uniform (Fig. 2). Also, the optical and radiation properties of the heat pipe surface are temperature dependent, and the effective radiation view factor for the outward facing surface is different than that for the inward facing surface because of the conical shape of the radiator. As a result, an accurate transient analysis of the SP-100 system's radiator heat pipes requires a three-dimensional transient model with capabilities for calculating the effective radiation view factor for each heat pipe and the surface emissivity as a function of temperature. Instead, the present two-dimensional model simulates the SP-100 radiator's heat pipes using an equivalent heat pipe with a circular cross section and interconnecting fins. As shown in Fig. 4, during normal operation, the portion of the heat pipe mounted onto the coolant duct is the evaporator region, while the rest of the heat pipe functions as the condenser region. The system's waste heat is transferred from the lithium in the secondary coolant ducts to the heat pipes, whose potassium working fluid transports the heat to the condenser region, where it is rejected into space by radiation.

Figures 5 and 6 show the calculated steady-state power throughput as well as the coolant and wall temperatures of the heat pipes in the SP-100 radiator panel during normal operation at 100 kWe. These calculations were conducted through the coupling of the heat pipe model to the integrated Space Nuclear Power System Analysis Model (SNPSAM-mode 2). This model is being developed and continuously upgraded to simulate the steady-state and transient operation of the SP-100 system.[2,13] As Fig. 5 indicates, the system's waste-heat rejec-

tion increases with the length of the heat pipe in the radiator panel, but it is higher for the heat pipes connected to the inlet (hot leg) secondary coolant duct than that for those connected to the return (cold leg) duct. Conversely, the results in Fig. 6 indicate that the surface temperature of the radiator's shortest heat pipe is higher than that of the longest heat pipe. However, the surface temperatures of the heat pipes connected to the hot leg of the secondary coolant duct are higher than those of the heat pipes connected to the cold leg of the duct.

The results presented in this paper are limited to the analysis of a single heat pipe, which was subjected to an external heat source on its inward facing surface (i.e., on the side opposite the coolant duct) (see Fig. 4). During the transient, although the bulk temperature T_b of the secondary lithium coolant was kept constant and equal to that during normal system operation (792 K), the wall temperature of the heat pipe was allowed to change with the external heating as well as with the net heat flow between the heat pipe and the secondary lithium coolant. Also, since the lithium flow rate in the secondary coolant duct during the system's nominal operation is low (0.8 kg/s), the heat-transfer coefficient for lithium is almost constant.[13] The axial temperature distribution in the heat pipe as well as the net heat flow between the heat pipe and the secondary lithium coolant were calculated as functions of time following an external thermal exposure. As shown in Fig. 5, the temperature drop across the composite wall of the SP-100 radiator heat pipe is less than 1 K. In the following section, the results of a parametric analysis investigating the transient responses of a radiator heat pipe to external thermal exposure are presented.

Results and Discussion

The geometrical and base-case parameters used in the analysis of the heat pipe's survivability to external heating are listed in Table 2. In this table, the exposed fraction x, is defined as the ratio of the exposed length to the total length of the heat pipe. The surface emissivity was taken to be constant and equal 0.85, and the effective radiation view factor of the inward facing surface was assumed constant (0.2) but smaller than that for the outward facing surface (0.95). However, these values may be different from actual values obtained by accurate calculations of the effective emissivity and the radiation view factor, which are beyond the scope of this investigation. Although these assumptions will affect the accuracy of the result, the parametric analysis should be useful in identifying the relative importance of various parameters on the transient operation of the radiator heat pipes.

In the base case analyzed, 50% of the total heat pipe length was subjected to a net external heat flux of 70 kW/m^2 for 10 s (see Table 2). The heat pipe was initially operating at a steady-state power throughput of 553 W. The calculated temperature distributions along the heat pipe are plotted in Fig. 7 for different times after the initiation of transient. As this figure shows, the heat pipe temperature was initially uniform along the whole length of the heat pipe at 776 K. However, the temperature in the region where the external heating is applied increased faster than that in the condenser region; the difference between these two temperatures decreased with time approaching a new steady state after about 10 s. As indicated in this figure, the new temperature distribution with an external heating of 23.3 kW/m^2, which corresponds to an external power input of 415 W, was uniform along the length of the heat pipe, indicating a continued forward operation of the heat pipe. However, at a higher external heat flux of 70 kW/m^2, the new steady-state temperature distribution shows that the temperature in the evaporator region is slightly lower than the temperatures in the condenser regions on both sides of the evaporator. This slight drop indicates a reversed operation of the heat pipe; in this case, the secondary coolant serves as a heat sink. Figure 7 also shows that the temperatures of the heat pipe increase slowly with the external heat flux. For example, an external heat flux of 23.3 kW/m^2 caused the heat pipe temperature to rise by only 11 K, from 776 to about 787 K. Also, increasing this external heat flux by 200% to 70 kW/m^2 increases the maximum heat pipe temperature to 809 K, only a 3% increase. This slow increase in the heat pipe temperatures with the external heat flux is because most of the external heating is either radiated into space or transmitted to the secondary lithium coolant in the duct.

Effect of Exposed Fraction

Because the heat rejection from the heat pipe occurs solely by radiation, increasing the heat pipe temperature increases the radiative heat-rejection capability of the heat pipe (broken lines in Figs. 8a and 9a), thus reducing the fraction of the external heat being transferred to the secondary lithium coolant (solid lines in Figs. 8a and 9a). When this fraction becomes approximately equal to the initial power transported from the coolant duct to the heat pipe, the heat pipe reverses its operation. In this case, the external heat exposure will be partially radiated into space and the rest transmitted by convection to the secondary lithium coolant. Although the rate of heat transfer to the coolant is directly proportional to the temperature differential between the heat pipe wall and the coolant, the radiation heat rejection increases proportionally to the wall temperature raised to the fourth power. To assess the contribution of these mechanisms to the survivability of

Table 2 Geometrical and base-case parameters of the radiator heat pipe

Geometrical parameters:	
Average length, m	0.735
Outer diameter, cm	1.651
Wall thickness, cm	0.0508
Annular thickness, cm	0.0508
Pore size, μ	40.0
Wall material	Ti over Be
Working fluid	K
Coolant duct width, cm	15.24
Coolant duct height, cm	0.8
Secondary coolant	Li
Base case parameters:	
Length of heat pipe, m	0.92
Exposed length L_{ex}, m	0.46
Exposed fraction x	0.5
Exposed time t_{ex}, s	10.0
External heat flux, kW/m^2	70.0
Initial input power P_o, W	553.0
Coolant bulk temperature T_b, K	792.0
Surface emissivity	0.85
Effective radiation view factor:	
Outward facing surface	0.95
Inward facing surface	0.20

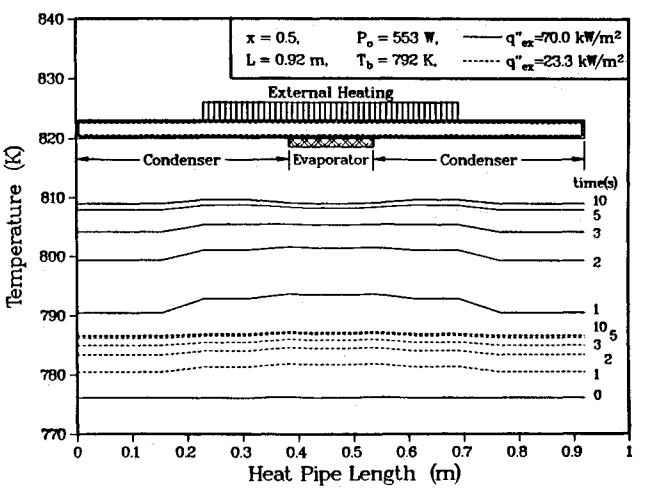

Fig. 7 Calculated axial temperature distributions in 0.92-m long heat pipe exposed to external heat fluxes of 23.3 and 70 kW/m^2.

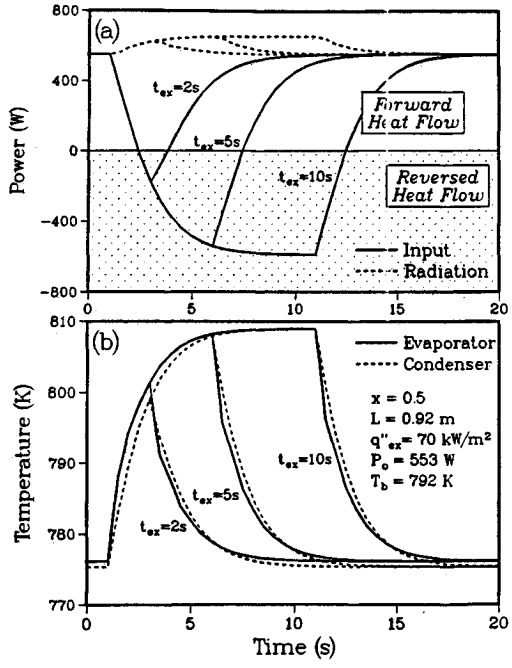

Fig. 8 Calculated temperature and power throughput for an exposed fraction of 0.5 and external heat flux of 70 kW/m².

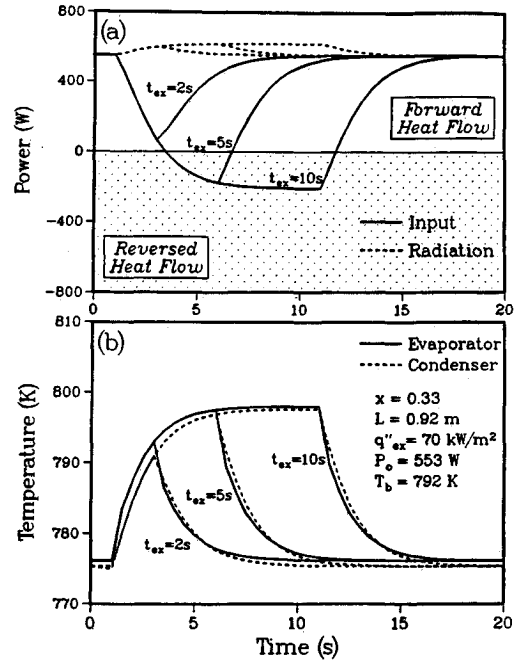

Fig. 9 Calculated temperature and power throughput for an exposed fraction of 0.33 and external heat flux of 70 kW/m².

the heat pipes to an external thermal exposure, parametric analyses were performed and the results are presented in Figs. 8–10. The base-case parameters in Figs. 8 and 9 are the same except for the exposed fraction; it is 0.5 and 0.33, respectively. In Fig. 10, the heat pipe is fully exposed to external heating at a significantly higher heat flux (200 and 400 kW/m²) than that in Figs. 8 and 9 (70 kW/m²).

As shown in Fig. 8a, the input power from the secondary lithium coolant to the heat pipe decreased rapidly and became negative about 2.5 s after the initiation of the transient. This negative input power indicates that the heat pipe operates in the reversed mode. When the exposure time was 2 s, the heat pipe reverted to a normal forward flow about 3.5 s after the initiation of the transient. The recovery time, as well as the time for incipient reversed operation, increases as the exposed fraction and/or the external heat flux increases (see Figs. 8–10). The recovery time is defined as the time between the end of the exposure and re-establishing the normal temperature of the heat pipe. As indicated in these figures, the heat pipe temperature reached 98% of its new steady-state value about 6.5 s after the initiation of the transient. This time was defined in this work as the response time of the heat pipe, t_{ss}.

Figures 8–10 also demonstrate that, for a given external heat flux, although increasing the exposure time does not change the time for incipient reversed operation of the heat pipe, it does increase the recovery time. In addition, for an exposure time shorter than the response time of the heat pipe (6.5 s), the fractions of the external heating radiated into space and transferred to the secondary lithium coolant simultaneously increase with exposure time. Beyond 6.5 s, however, these fractions reached asymptotic values that depend on the external heat flux and the exposed fraction. As indicated in Fig. 8, for an external heat flux of 70 kW/m² and an exposed fraction of 0.5, the maximum forward heat flow was 647 W and the maximum reversed heat flow was 597 W, giving that the maximum fractions of the external heating radiated into space and transported to the secondary coolant duct are 52 and 48%, respectively. However, when the exposed fraction was decreased from 0.5 to 0.33 (or the external power from 1244 to 821 W), the maximum fraction of the external heating that is rejected by radiation into space increased to as high as 72% (see Fig. 9).

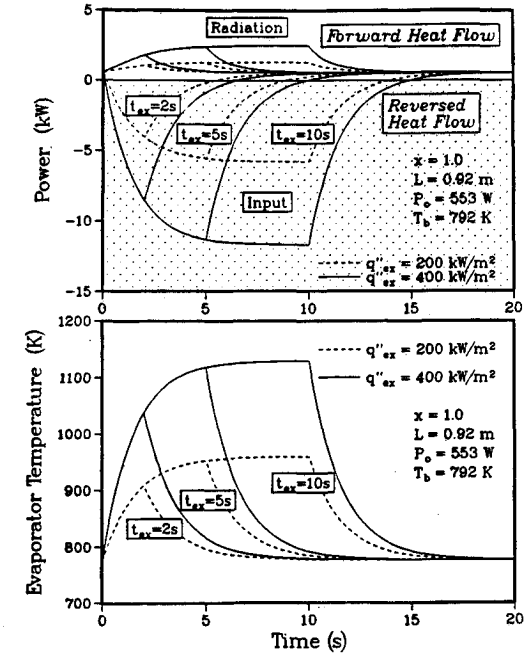

Fig. 10 Calculated temperature and power throughput for a fully exposed heat pipe to external heat fluxes of 200 and 400 kW/m².

Effect of External Heat Flux

Figure 10 shows that increasing the external heat flux significantly increases both the fraction of external heating transported to the secondary lithium coolant and the recovery time of the heat pipe, but decreases the time for incipient reversed operation. For a fully exposed heat pipe, doubling the external heat flux from 200 to 400 kW/m² increased the maximum fraction of external heat transported to the secondary lithium coolant from 80 to 84%, but reduced the time for incipient reversed operation from 0.2 to 0.1 s. These results, as well as those presented in Figs. 8 and 9, demonstrate that although increasing either the external heat flux or the exposed fraction increases the heat pipe temperature and the total heat rejection by radiation, it reduces the fraction of the external heat radiated into space, resulting in a significant heating of the sec-

ondary lithium coolant. These results could have significant effects on the vulnerability of the SP-100 system to external heating of its radiator.

The results in Fig. 10 demonstrate that a full exposure of the radiator heat pipe to net heat flux of only 200 kW/m^2 for more than 6.5 s could cause the heat pipe wall to fail as the induced stress in the wall due to the potassium vapor pressure exceeds the yield strength of the titanium liner in the wall. At such heat flux the wall temperature increases to as high as 960 K, which is only 271 K below the melting temperature of the silver bonding layer in the wall. Also, at 960 K, the vapor pressure of the potassium working fluid in the heat pipe (about 0.053 MPa) induces tangential stress in the titanium liner (about 3.9 MPa) which exceeds the yield strength of the titanium at this temperature. Figure 10 also shows that increasing the net heat flux to 400 kW/m^2 increases the heat pipe wall temperature to 1130 K, which is the only 65 K below the melting temperature of the silver bonding layer.

Figures 11 and 12 plot the effects of the external heat flux and exposure time on the duration of reversed operation of the heat pipe. As these figures show, the minimum value of the net external heat flux needed to reverse the operation of the heat pipe strongly depends on the exposed fraction; it is about 31 and 51 kW/m^2 for exposed fractions of 0.5 and 0.33, respectively, and as low as 17 kW/m^2 for a fully exposed heat pipe (see Fig. 12). These heat-flux values approximately correspond to an external power of 533 W, which is the same as the initial power throughput P_o of the heat pipe. For external heat fluxes higher than these values, the time at which reversed operation occurs decreases as the external heat flux increases. Also, the duration of reversed operation increases with the increase in either the external heat flux or the exposure time. As shown in Figs. 11 and 12, when the exposed fraction decreases from 1.0 to 0.33, the boundary of the area for reversed operation shifts to the right, toward the higher external heat flux. These figures also show that, for an exposure time of 2.0 s, the reversed operation for 0.33 exposed fraction begins at an external heat flux of 80 kW/m^2, which is about 50 and 240% higher than those with 0.5 exposed fraction and fully exposed heat pipe, respectively.

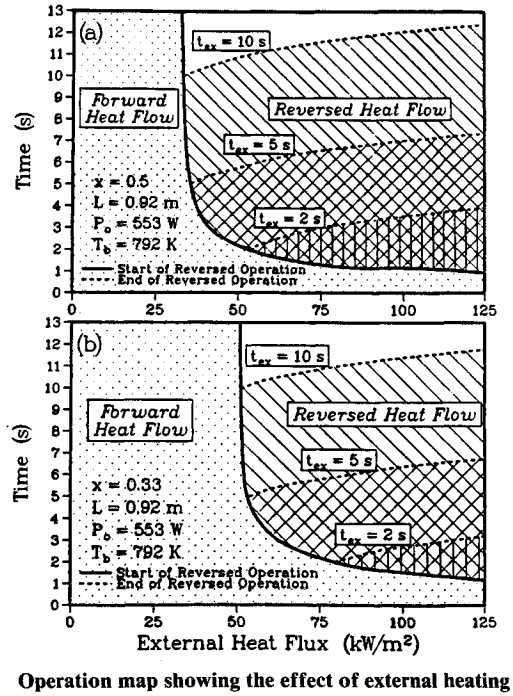

Fig. 11 Operation map showing the effect of external heating on the operation of a radiator heat pipe with exposed fractions of 0.5 and 0.33.

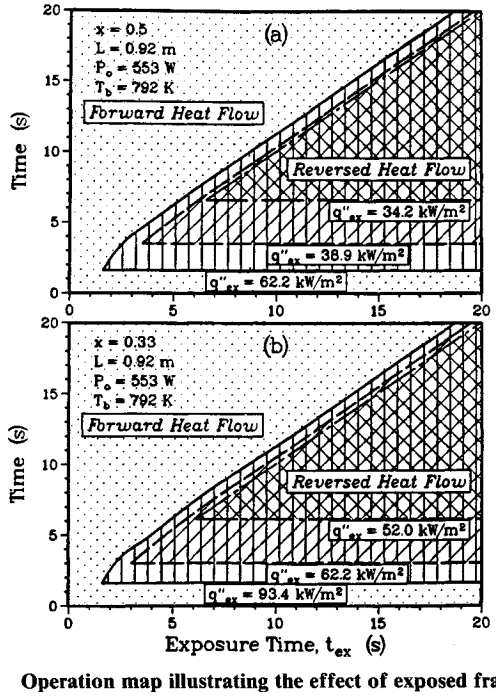

Fig. 13 Operation map illustrating the effect of exposed fraction on the operation of a radiator heat pipe exposed to external heating.

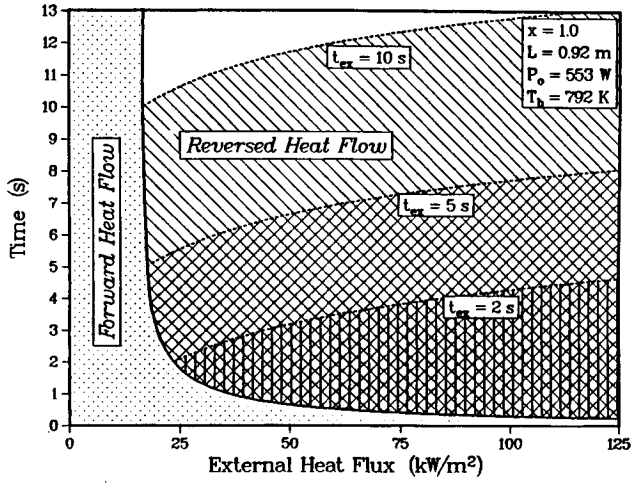

Fig. 12 Operation map of a fully exposed radiator heat pipe showing the effect of external heating.

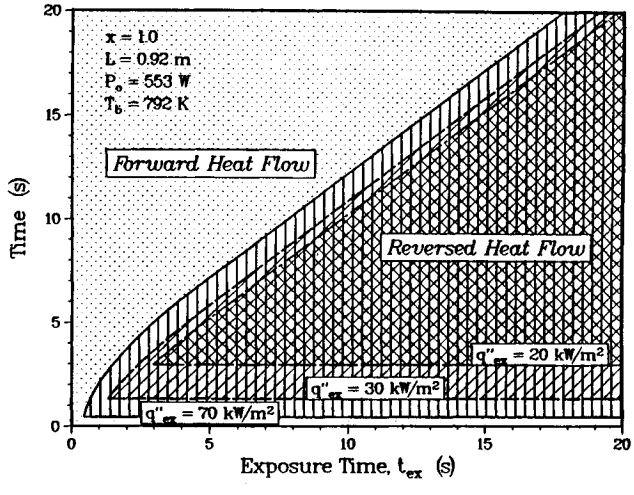

Fig. 14 Operation map of a fully exposed radiator heat pipe illustrating the effect of exposure time.

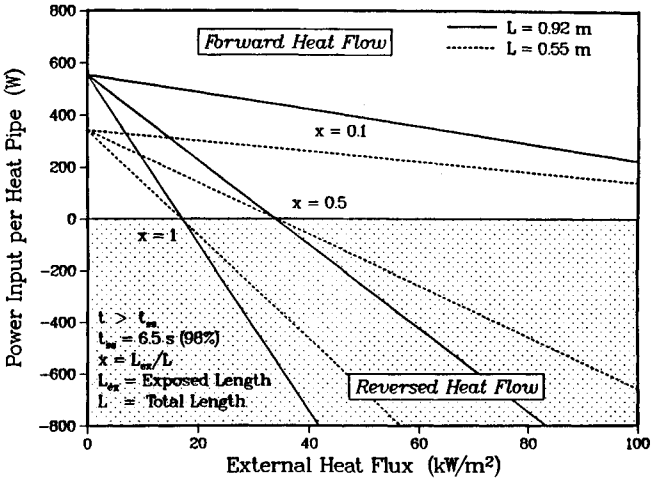

Fig. 15 Effects of external heat flux and exposed fraction of radiator heat pipes on the power throughput for exposure times greater than the heat pipe's response time (~ 6.5 s).

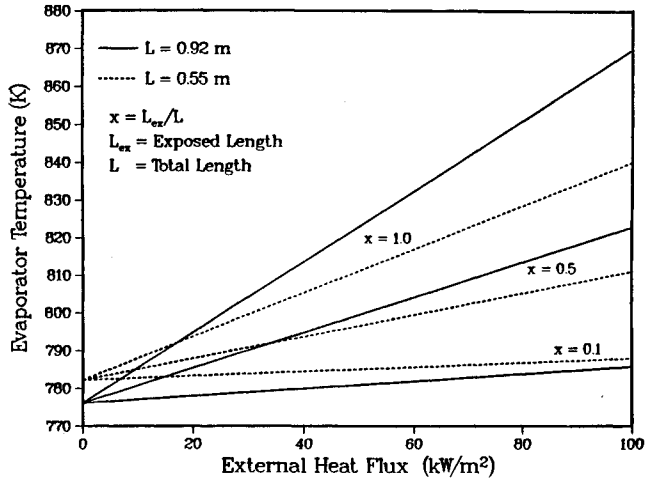

Fig. 16 Effects of external heat flux and exposed fraction on the heat pipe evaporator temperature.

Effect of Exposure Time

Figures 13 and 14 show the duration of reverse operation of the radiator heat pipe as a function of the exposure time for different external heat fluxes and exposed fractions. As shown in these figures, for a given external heat flux, the time for incipient reversed operation of the heat pipe is independent of the exposure time; however, the duration of reverse operation increases as the exposure time increases. The recovery time also increases with external heat flux and the exposure time. Figure 13 indicates that, for an external heat flux of 62.2 kW/m^2, reducing the exposed fraction (from 0.5 to 0.33) increases the time for incipient reversed operation but reduces the duration of reversed operation. This decreased duration of reversed operation occurs because decreasing the exposed fraction, at the same external heat flux, reduces the external power input to the heat pipe during the transient (from 1106 to 730 W for x of 0.5 and 0.33, respectively), resulting in a shorter recovery time.

Transient Operation of Radiator Heat Pipe for $t > t_{ss}$

Figures 15–17 present the effect of external heat flux on the operation of the radiator heat pipe for exposure times that are longer than the response time of the heat pipe ($t > t_{ss}$), where t_{ss} = 6.5 s. Figures 15 and 16 plot the calculated power throughput of the heat pipe and the evaporator temperature as functions of the external heat flux and the exposed fraction. The heat pipe lengths of 0.92 and 0.55 m used in this analysis

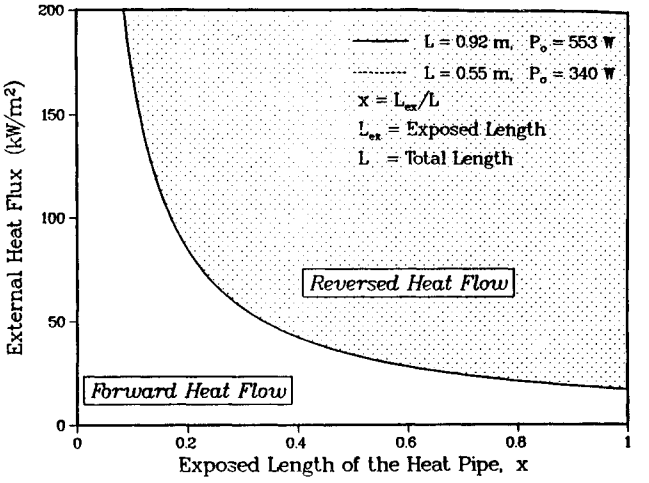

Fig. 17 Operation map for radiator heat pipes exposed to external heating for exposure times greater than the heat pipe's response time (~ 6.5 s).

represent the longest and shortest heat pipes in the SP-100 radiator panel, respectively. As these figures indicate, during normal system operation (i.e., zero external heat flux), the power throughput from the secondary coolant duct to the radiator heat pipes was higher for the longest heat pipe, but the evaporator temperature was slightly lower then that for the shortest heat pipe (see also Figs. 5 and 6). These differences in the power throughput and temperature between the radiator's longest and shortest heat pipe are caused by the difference in the condenser area. The longer heat pipe has a larger condenser area, which results in a lower wall temperature but higher heat-rejection capability than those for the shorter heat pipe. The ratio of the steady-state power throughput in the longest and the shortest heat pipes in the radiator can be written as

$$\frac{P_l}{P_s} = \left(\frac{L_l}{L_s}\right)\left(\frac{\epsilon_l F_l}{\epsilon_s F_s}\right)\left(\frac{T_l}{T_s}\right)^4 \tag{1}$$

Because of T^4, the SP-100 sink temperature of 250 K can be left out from the equation only for high-temperature radiator ($T > 750$ K). Assuming the same surface emissivity and radiation view factor for the longest and the shortest heat pipes in the SP-100 radiator panel, substituting the evaporator temperatures and the heat pipe lengths into Eq. (1) gives a power ratio of 1.62. This ratio is the same as that which can be deduced from Fig. 15, where P_l and P_s are 553 and 340 W, respectively. However, since the longest and shortest heat pipes in the panel operate at different surface temperatures and consequently different emissivities as well as have different radiation view factors, the actual power ratio will be different that that given in Fig. 15. As indicated earlier, future work may quantify the effects of the different surface emissivity and radiation view factor on the radiator performance.

During an external thermal exposure at the same heat flux, the total external power input to the radiator's heat pipe is also proportional to its total length and exposed fraction. Because the net power exchange between the heat pipe and the secondary coolant duct is zero at the point of incipient reversed operation (or zero input power), all of the external power input is rejected into space by radiation. Therefore, assuming constant emissivity and radiation view factor, the ratio of the external heat flux for the longest and shortest heat pipes in the radiator panel at a fixed heat flux can be given as

$$\left(\frac{q''_l}{q''_s}\right) = \left(\frac{x_s}{x_l}\right)\left(\frac{T_l}{T_s}\right)^4 \tag{2}$$

This equation indicates that, for the same exposed fraction (i.e., $x_l = x_s$) and the same evaporator temperatue ($T_l = T_s$),

the external heat flux for incipient reversed operation of the radiator heat pipes will be the same, regardless of the length of the heat pipe. It can easily be shown that Eq. (2) applies to the point of zero power input in Figs. 15 and 16. As these figures demonstrate, at the point of incipient reversed operation (or zero input power), the external heat flux and the evaporator temperature were the same for the same exposed fraction of both the longest and the shortest heat pipes. Beyond this point, the evaporator temperature and the power transferred from the heat pipe to the coolant duct for the longest heat pipe were higher than those for the shortest heat pipe. The results in Figs. 15 and 16 also show that increasing the external heat flux beyond the point of incipient reversed operation not only increases the heat flow rate from the heat pipe to the lithium coolant in the secondary duct (see Fig. 4) but also raises the evaporator temperature. Figure 15 indicates that, for a given exposed fraction, the input power for the longest heat pipe decreases more rapidly with the external heat flux than that for the shortest heat pipe.

Figure 17 presents a transient operation map of the radiator heat pipes for exposure times greater than the heat pipe's response time (i.e., $t > t_{ss}$). As this figure indicates, the external heat flux needed to cause a reversed operation is independent of the total length of the heat pipe; however, it decreases as the exposed fraction increases. The results in Fig. 17 also show that, for a fully exposed radiator panel (i.e., $x = 1.0$), the minimum external heat flux needed to reverse the operation is as low as 17 kW/m^2. Although this heat flux is well below the 590 kW/m^2 required to adiabatically heat the pipe's beryllium overcoating to its melting point (1552 K), it will bring the waste-heat rejection of the radiator panel to a halt.

Summary and Conclusions

This research investigated the transient response of a potassium heat pipe, simulating those of the SP-100 system's radiator heat pipes, to an external thermal exposure. The results showed that a heat pipe failure caused by an external heating below 200 kW/m^2 is unlikely; a reversed operation that will transport a fraction of the external heat to the lithium in the secondary coolant will temporarily occur. This fraction of the external heat increases with the external heat flux, the exposed fraction of the heat pipe, and the exposure time up to the heat pipe's response time (~ 6.5 s). Beyond this time, the heat pipe reaches steady state where the fraction of the external heat transported to the secondary coolant becomes independent of the exposure time. Conversely, the fraction of the external heat radiated into space decreases as the exposed fraction of the heat pipe and/or the external heat flux increases.

Results indicated that, for exposure times shorter than the response time of the heat pipe (~ 6.5 s), a full exposure of as low as 17 kW/m^2 can reverse the operation of the heat pipe, regardless of its length. The duration of reversed operation depends on the external heat flux and the exposure time, as well as the exposed fraction and the total length of the heat pipe. For exposure times longer than the response time of the heat pipe (~ 6.5 s), increasing the exposed fraction reduces the external heat flux required to reverse the heat pipe operation. However, for a given exposed fraction, the external heat flux required to reverse the operation of the radiator heat pipe is independent of the total length of the heat pipe.

Results also demonstrated that a full exposure of the SP-100 radiator heat pipes to a net heat flux of only 200 kW/m^2 for more than 6.5 s could cause the heat pipe wall to fail as the induced stress in the wall due to the vapor pressure of the potassium working fluid exceeds the yield strength of the titanium liner. Increasing the external heat flux from 200 to 400 kW/m^2 increases the wall temperature from 960 to 1130 K, which is only 65 K below the melting point of the silver-bonding layer in the heat pipe wall.

Acknowledgment

This research is funded by the Institute for Space Nuclear Power Studies, Chemical and Nuclear Engineering Department, University of New Mexico, Albuquerque, New Mexico.

References

[1]Wiltshire, F., Kaplan, S., Lunsford, D., O'Neil, G., Otwell, R., and Plumlee, D., "SP-100 Reactor Design," *Transactions of the 5th Symposium on Space Nuclear Power Systems,* Institute for Space Nuclear Power Studies, Univ. of New Mexico, Albuquerque, NM, Jan. 1988.

[2]Seo, J. T., "Transient Analysis of Space Nuclear Power Systems," Ph.D. Dissertation, Dept. of Chemical and Nuclear Engineering, The Univ. of New Mexico, Albuquerque, NM, May 1988.

[3]Seo, J. T. and M. S. El-Genk, "A Transient Model for Liquid Metal Heat Pipes," *Transactions of the 5th Symposium on Space Nuclear Power Systems,* Institute for Space Nuclear Power Studies, Univ. of New Mexico, Albuquerque, NM, Jan. 1988, pp. 114–119.

[4]Seo, J. T. and M. S. El-Genk, "A Transient Model for Liquid Metal Heat Pipes," *Space Nuclear Power Systems 1988,* edited by M. S. El-Genk and M. D. Hoover, Orbit, Malabar, FL, 1988, in press.

[5]Bowman, W. J. and Hitchcock J., "A Compressible Vapor Flux Model for Transient Heat Pipe Analysis," *Transactions of the 4th Symposium on Space Nuclear Power Systems,* CONF-870102-Summs, Institute for Space Nuclear Power Studies, Univ. of New Mexico, Albuquerque, NM, Jan. 1987, pp. 358–388.

[6]Costello, F. A. et al., "Detailed Transient Model of a Liquid-Metal Heat Pipes," *Transactions of the 4th Symposium on Space Nuclear Power Strategies,* CONF-870102-Summs, Institute for Space Nuclear Power Studies, Univ. of New Mexico, Albuquerque, NM, Jan. 1987, pp. 393–402.

[7]Peery, J. S. and Best, F. R., "Simulation of Heat Pipe Rapid Transient Performance Using a Multi-Nodal Implicit Finite Difference Scheme," *Transactions of the 3rd Symposium on Space Nuclear Power Systems,* CONF-860102-Summs, Institute for Space Nuclear Power Studies, Univ. of New Mexico, Albuquerque, NM, Jan. 1986, pp. TM 4.1-TM 4.3.

[8]Cullimore, B. A., "Modeling of Transient Heat Pipe Effects Using a Generalized Thermal Analysis Program," Transient Heat Pipe Modeling Workshop, Institute for Space Nuclear Power Studies, Univ. of New Mexico, Los Alamos, NM, March 1986.

[9]Chang, W. S. and Colwell, G. T., "Mathematical Modeling of the Transient Operating Characteristics of a Low-Temperature Heat Pipe," *Numerical Heat Transfer,* Vol. 8, 1985, pp. 169–186.

[10]Ransom, V. H. and Chow, H., "ATHENA Heat Pipe Transient Model," *Transactions of the 4th Symposium on Space and Nuclear Power Systems,* CONF-870102-Summs, Institute for Space Nuclear Power Studies, Univ. of New Mexico, Albuquerque, NM, Jan. 1987, pp. 389–392.

[11]Hall, M. L. and Doster, J. M., "Transient Thermohydraulic Heat Pipe Modeling," *Transactions of the 4th Symposium on Space Nuclear Power Systems,* CONF-870102-Summs, Institute for Space Nuclear Power Studies, Univ. of New Mexico, Albuquerque, NM, Jan. 1987, pp. 307–410.

[12]Merrigan, M. A., Keddy, E. S., and Sena, J. T., " Transient Performance Investigation of a Space Power System Heat Pipe," AIAA Paper 86-1273, June 1986.

[13]El-Genk, M. S. and Seo, J. T., "SNPSAM – Space Nuclear Power System Analysis Model," *Space Nuclear Power Systems 1986,* edited by M. S. El-Genk and M. D. Hoover, Orbit, Malabar, FL, 1987, pp. 111–133.